Dual-Mode GVD Tailoring in a Convex Waveguide
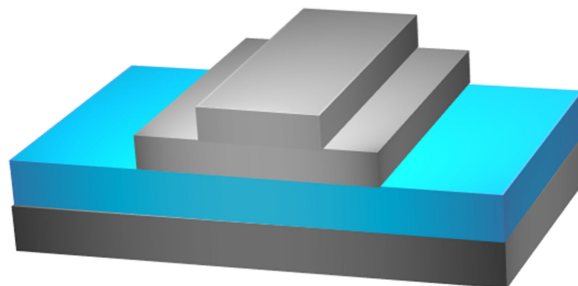
Weicheng Chen, *Student Member, IEEE*
Gongcheng Yue, *Student Member, IEEE*
Haofeng Hu
Zhenzhou Cheng, *Senior Member, IEEE*
Guo-Wei Lu
Tiegen Liu

Dual-Mode GVD Tailoring in a Convex Waveguide

Weicheng Chen [ORCID],[1,2] *Student Member, IEEE*,
Gongcheng Yue [ORCID],[1] *Student Member, IEEE*, Haofeng Hu [ORCID],[1,2]
Zhenzhou Cheng [ORCID],[1,2,3] *Senior Member, IEEE*, Guo-Wei Lu [ORCID],[4,5]
and Tiegen Liu[1,2]

[1]School of Precision Instruments and Optoelectronics Engineering, Tianjin University,
Tianjin 300072, China
[2]Key Laboratory of Optoelectronics Information Technology, Ministry of Education, Tianjin
300072, China
[3]Department of Chemistry, The University of Tokyo, Tokyo 113-0033, Japan
[4]National Institute of Information and Communications Technology, Tokyo 184-8795, Japan
[5]The University of Aizu, Fukushima 965-8580, Japan

Abstract: Mode division multiplexing (MDM) silicon photonic integrated circuits (PICs) have been widely developed for achieving high-speed optical interconnects and communications. As an excellent nonlinear optical platform, silicon PICs also receive great attention in applications of optical parametric devices and nonlinear optical signal processing. However, it is still challenging to develop MDM optical parametric devices due to the strong mode dependence of the group velocity dispersion (GVD) in a silicon waveguide. Here, we theoretically design a convex waveguide exhibiting almost the same GVD profiles for quasi-TE$_0$ and quasi-TE$_1$ modes based on the standard fabrication flow of silicon photonic foundries. Specifically, flat GVD curves varying from -1500 ps/nm/km to -1000 ps/nm/km are obtained for the two modes in a convex waveguide within a spectral region of 1.37 μm to 1.75 μm covering from E-band to U-band. The study is expected to open an avenue for exploring unprecedented MDM nonlinear applications.

Index Terms: Silicon waveguide, nonlinear optics, guided waves.

1. Introduction

Mode division (de)multiplexing (MDM) silicon photonic integrated circuits (PICs) have great potential for scaling the bandwidth of optical interconnects and communications [1], [2]. In such technique, spatial orthogonal modes in a multimode waveguide are utilized as distinct information channels, providing an additional degree of freedom to boost information capacity of optical networks together with other (de)multiplexing techniques, such as time division (de)multiplexing [3], wavelength division (de)multiplexing [4] and polarization division (de)multiplexing [5]. By taking this advantage, high-speed optical interconnects with a data rate of 10.68 Tb/s have been demonstrated to date [6]. Also, MDM PICs have been widely demonstrated in applications of on-chip optical transceivers [7] optical switching [8], and optical routing [9].

(a)

Width (W)

Top Silicon Thickness

BOX

Silicon Substrate

(b)
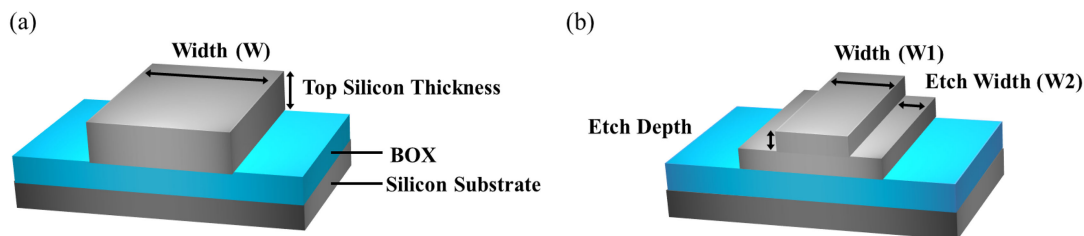
Width (W1)

Etch Width (W2)

Etch Depth

Fig. 1. Schematics of the dual-mode silicon waveguides. (a) Channel waveguide. The channel waveguide was designed on the commercial SOI wafer with the 220-nm-thick top silicon layer and 2-μm-thick BOX. (b) Convex waveguide. The symmetrical stepped structures were designed on the two edges of the channel waveguide to achieve the GVD engineering for both quasi-TE$_0$ and quasi-TE$_1$ modes.

On the other hand, silicon PICs have received great attention in developing optical parametric devices [10]–[12] and nonlinear optical signal processing [13], due to the high intrinsic Kerr nonlinearity of silicon material which is up to 2.6 $\times$ 10^{-18} m^2/W at a wavelength of 1550 nm [14], [15]. Besides, the flexible group velocity dispersion (GVD) engineering is also inevitable to achieve high-efficiency and broadband optical parametric applications in a silicon waveguide [16]–[18]. Previous studies show that through tailoring structures of silicon waveguides, it is possible to obtain a flat anomalous GVD profile in an ultrawide spectral region, for supporting uniform multiple wavelength operations [19]–[22]. As a result, many efforts have been made to demonstrate on-chip optical frequency combs [23], supercontinuum generation [24], signal parametric amplification and regeneration [25] under a single spatial mode. Moreover, for the MDM nonlinear wavelength conversion studies [26], it could be helpful to achieve similar conversion efficiencies and spectral bandwidths for the quasi-TE$_0$ and quasi-TE$_1$ modes if the two modes have almost the same GVD profiles in the waveguide. However, it is still challenging to develop MDM optical parametric devices and applications due to the mode dependence of the GVD in a silicon waveguide. It can be expected that a multi-mode waveguide with flat and overlap GVD profiles for all spatial modes could be useful for achieving MDM optical parametric devices. To date, the study of GVD tailoring for multiple modes is still in its infant, to the best of our knowledge.

In this paper, we design a convex waveguide based on the standard fabrication flow of silicon photonics foundries to obtain flat dual-mode GVD profiles. The method is based on the exploration of the influence of the convex waveguide structure on the GVD of two spatial modes. To be specific, flat GVD curves varying from −1500 ps/nm/km to −1000 ps/nm/km are obtained for the quasi-TE$_0$ and quasi-TE$_1$ modes in the convex silicon waveguide within a spectral region of 1.37 μm to 1.75 μm covering from E-band to U-band. Moreover, our design is fully compatible with commercial foundry services, making it possible to fabricate the convex waveguides in an appreciable-quality, high-density, and low-cost way. Our study is expected to open an avenue for exploring unprecedented MDM optical parametric devices and nonlinear optical signal processing applications on a chip.

2. Design Principle and GVD Tailoring

In this work, we studied and compared a dual-mode channel waveguide and dual-mode convex waveguide, as schematically shown in Fig. 1. The waveguides were designed based on a commercial silicon-on-insulator (SOI) wafer, which has a 220-nm-thick top layer silicon layer and 2-μm-thick buried oxide (BOX). As for the channel waveguide, we studied effective refractive indices (RIs) and GVD curves with different waveguide widths, as shown in Fig. 1(a). While for the convex waveguide, symmetrical stepped structures were designed on two edges of a channel waveguide to achieve GVD engineering for both quasi-TE$_0$ and quasi-TE$_1$ modes, as shown in Fig. 1(b). Since the stepped structures exert more influence on the RI of the quasi-TE$_1$ mode than that of the quasi-TE$_0$ mode, it may be possible to have additional degrees of freedom to engineer the GVD curves for the
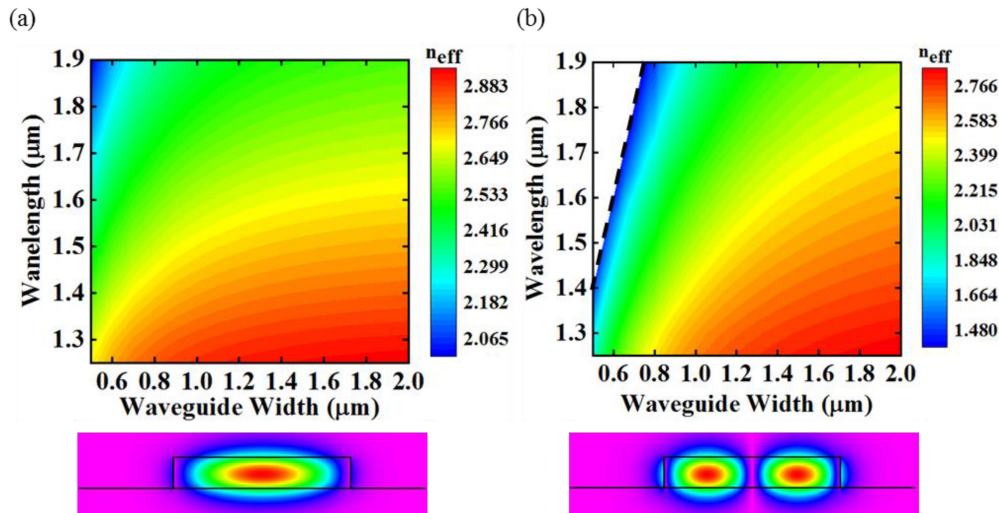
Fig. 2. Effective RIs of quasi-TE_0 and quasi-TE_1 modes in the channel waveguide as a function of the waveguide width and wavelength, and electric-field magnitude distributions of the waveguide cross-section. (a) Quasi-TE_0 mode. (b) Quasi-TE_1 mode.

two spatial modes in the convex waveguide. In our design, we chose two etching depths, namely, 70 nm and 150 nm, and different waveguide widths and etch widths to calculate effective RIs and GVD curves. It is worthwhile to note that the wafer structure and etching depths in our design are fully compatible with commercial foundry services, namely, imec's silicon photonics passive and active platforms, making it possible to fabricate the convex waveguides in an appreciable-quality, high-density, and low-cost way.

We first simulated waveguide effective RIs by using a full-vector mode solver based on the beam propagation method providing by commercial software (Rsoft Photonic Device Tool), and then calculated GVD curves based on the simulated results. The effective RIs of the quasi-TE_0 and quasi-TE_1 modes of the channel waveguide as a function of the waveguide width and wavelength are shown in Figs. 2(a) and (b). We changed the channel waveguide width from 0.5 μm to 2 μm and the wavelength from 1.25 μm to 1.9 μm in our modal. Both the quasi-TE_0 mode and quasi-TE_1 mode exhibit similar effective RI change trends by increasing the waveguide width and wavelength. While, there are cutoff wavelengths for the quasi-TE_1 mode when reducing the waveguide width, as indicated by the black dash line in Fig. 2(b). The GVD characteristics of quasi-TE_0 and quasi-TE_1 modes could be calculated by using the GVD formula [20],

$$D = - (\lambda/c) \, d^2 n_{\text{eff}}/d\lambda^2, \tag{1}$$

where D is the GVD, λ is the wavelength, c is the light velocity in a vacuum, n_{eff} is the effective RI. It is well known that the total GVD includes material dispersion and waveguide dispersion. In our calculation, silicon material dispersion has been taken into account by using Sellmeier equations when simulating the waveguide effective RIs. While the total GVD was calculated based on the simulated results by using Eq. 1.

Based on the simulated effective RIs, we calculated the GVD curves of the quasi-TE_0 and quasi-TE_1 modes in the channel waveguide with waveguide widths (W) of 0.8 μm, 1.3 μm, 1.8 μm in the spectral region of 1.25 μm to 1.9 μm. As shown in Fig. 3, by controlling the geometric morphology of the waveguide, we could tailor the GVD profiles of the two spatial modes via engineering the light confinement in the channel waveguide. In the case of W = 0.8 μm, the GVD of the quasi-TE_1 mode first increases from 0 ps/nm/km to 1590 ps/nm/km, then steadily decreases to -5370 ps/nm/km, as shown in Fig. 3(a). While the GVD variation of the quasi-TE_0 mode is moderate compared with that of the quasi-TE_1 mode. By increasing waveguide width, the quasi-TE_0 and quasi-TE_1 modes
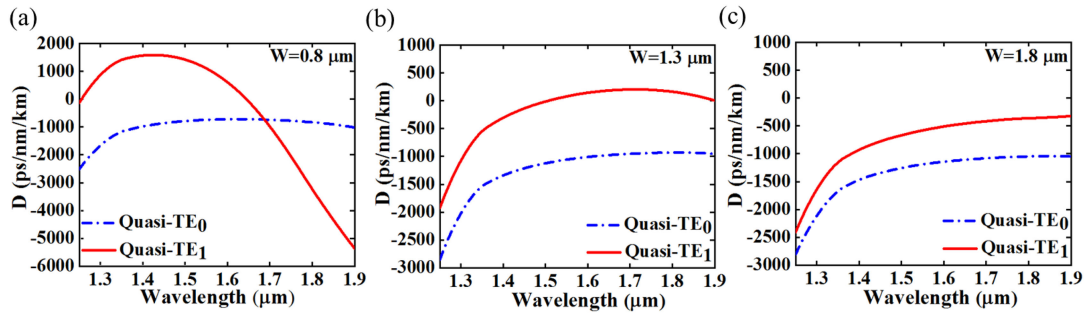
Fig. 3. GVD curves of the quasi-TE$_0$ and quasi-TE$_1$ modes in the channel waveguides with W = 0.8 μm, 1.3 μm, and 1.8 μm (a) GVD curves with W = 0.8 μm. The GVD of the quasi-TE$_0$ mode is flatter than that of the quasi-TE$_1$ mode. (b) GVD curves with W = 1.3 μm. The GVD of the quasi-TE$_0$ mode is smaller than that of the quasi-TE$_1$ mode, while the GVD profiles of the two modes are similar. (c) GVD curves with W = 1.8 μm. The GVD curves of the two spatial modes cannot overlap with each other, even increasing the W to 2.3 μm.
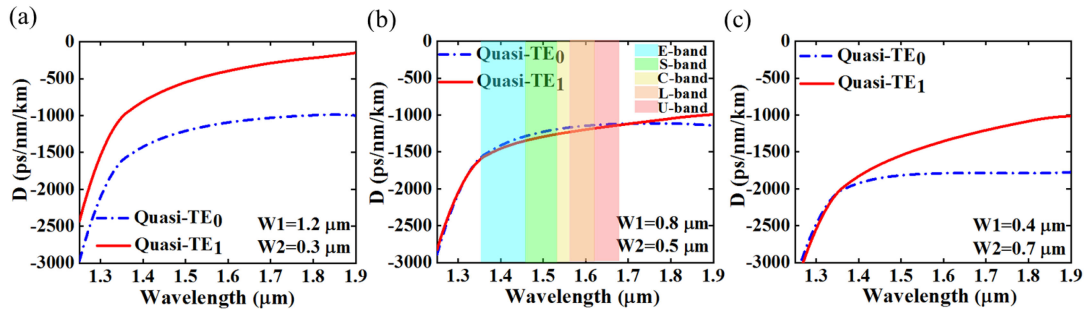

Fig. 4. GVD curves of the quasi-TE$_0$ mode and quasi-TE$_1$ mode in the convex waveguides with the etching depth of 70 nm. (a) GVD curves with W1 = 1.2 μm and W2 = 0.3 μm. The GVD curves of the quasi-TE$_0$ mode and quasi-TE$_1$ mode are similar to those in Fig. 3(c). (b) GVD curves with W1 = 0.8 μm and W2 = 0.5 μm. The GVD curves of the quasi-TE$_0$ mode and quasi-TE$_1$ mode overlap well with each other. (c) GVD curves with W1 = 0.4 μm and W2 = 0.7 μm. Compared with quasi-TE$_1$ mode, the GVD curve of the quasi-TE$_0$ mode dramatically decreases when the wavelength is beyond 1.4 μm.

have similar GVD profiles, as shown in Figs. 3(b) and 3(c). Then it may be easy to tailor the GVD profiles further to make them overlap with each other by shaping the waveguide structure. Therefore, in the following part, we fixed the waveguide width of 1.8 μm. For the on-chip MDM nonlinear wavelength conversion applications [26], a waveguide with almost the same GVD profiles for different spatial modes may be useful to achieve similar conversion efficiencies and spectral bandwidths. However, our numerical study shows that it is challenging for two spatial modes in a silicon channel waveguide, as the GVD curves of the two spatial modes could not overlap with each other by even accurately optimizing the waveguide width of the channel waveguide.

To achieve the similar GVD profiles for the quasi-TE$_0$ and quasi-TE$_1$ modes, we designed the convex waveguide based on the waveguide structure used in Fig. 1(b). The total waveguide width (W1 + 2 × W2) and etching depth were fixed as 1.8 μm and 70 nm in the convex waveguide, while we chose three waveguide structures, namely, W1 = 1.2 μm W2 = 0.3 μm, W1 = 0.8 μm W2 = 0.5 μm, and W1 = 0.4 μm W2 = 0.7 μm. We calculated the GVD curves of the quasi-TE$_0$ and quasi-TE$_1$ modes in the convex waveguide within the spectral region of 1.25 μm to 1.9 μm, as shown in Fig. 4(a)–(c). Compared with the quasi-TE$_0$ mode, the stepped structures in the convex waveguide have a larger spatial overlap with the quasi-TE$_1$ mode, thus we could tailor the GVD of the quasi-TE$_1$ mode without obviously changing the GVD of the quasi-TE$_0$ mode.
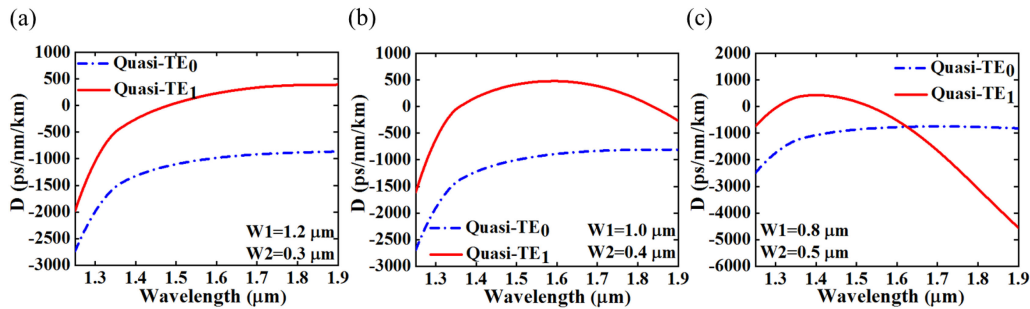
Fig. 5. GVD curves of quasi-TE$_0$ mode and quasi-TE$_1$ mode in the convex waveguides with the etching depth of 150 nm. (a) GVD curves with W1 = 1.2 μm and W2 = 0.3 μm. (b) GVD curves with W1 = 0.8 μm and W2 = 0.5 μm. (c) GVD curves with W1 = 0.4 μm and W2 = 0.7 μm. Compared with the waveguide design in Fig. 4, there are only 70-nm-thick slabs in this convex waveguide, so light is mainly confined in the center part of the waveguide for the quasi-TE$_0$ and quasi-TE$_1$ modes, resulting in the channel-waveguide-like GVD profiles.

With a proper design, the waveguide can support two spatial modes exhibiting almost identical GVD profiles, as shown in Fig. 4(b). In the spectral region of 1.37 μm to 1.75 μm, the GVD curves are extremely flat only varying from −1500 ps/nm/km to −1000 ps/nm/km. This feature provides us great potential in broadband nonlinear optical applications covering from E-band to U-band, as indicated in Fig. 4(b). The etching depth of 70 nm in our design is compatible with the standard silicon photonics fabrication flow of the imec [27]. It is worthwhile to mention that the convex waveguide may also be applicable for the dual-mode GVD engineering at the spectral region beyond 2 μm. Moreover, we simulated dual-mode GVD profiles by shifting an exposure alignment of 30 nm as well as changing an etching depth of 5 nm and etching width of 20 nm. The simulation results show that the design has good tolerance to the fabrication uncertainties. In the following part, we will also check the GVD profiles of the two spatial modes in the convex waveguide with another etching depth (150 nm) in the imec's standard fabrication process.

Finally, we studied the GVD curves of the quasi-TE$_0$ and quasi-TE$_1$ modes in the convex waveguide with the etching depth of 150 nm. Similarly, we chose three waveguide structures with a fixed width (W1 + 2 × W2) of 1.8 μm and calculated the GVD curves of the two spatial modes in the convex waveguide within the spectral region of 1.25 μm to 1.9 μm, as shown in Fig. 5(a)–(c). As shown in Fig. 5(a), with W2 = 0.3 μm the GVD profiles are similar to those in Fig. 4(a). While, by further increasing the W2, we cannot achieve similar GVD profiles for the quasi-TE$_0$ and quasi-TE$_1$ modes in the convex waveguide with the etching depth of 150 nm. Moreover, with W2 = 0.5 μm the GVD of the quasi-TE$_1$ mode shows a parabolic-like shape and has anomalous dispersion at 1.4 μm wavelengths, which is similar to the curve in Fig. 3(a). The explanation for these theoretical results is that the light confinement in the convex waveguide with the etching depth of 150 nm is similar to that in the channel waveguide. Since only 70-nm-thick slabs exist in the convex waveguide, most light is confined in the center part of the waveguide both for the two spatial modes. As a result, a proper etching depth is critical to design the convex waveguide for dual-mode GVD tailoring.

3. Conclusions

In conclusion, we theoretically studied the convex waveguide for dual-mode GVD tailoring. Based on the standard silicon photonics foundry service, we designed the convex waveguide which has almost identical GVD profiles for the quasi-TE$_0$ and quasi-TE$_1$ modes. Within the spectral region of 1.37 μm to 1.75 μm, we theoretically achieved flat GVD curves varying from −1500 ps/nm/km to −1000 ps/nm/km for the two spatial modes. Our study is expected to open an avenue for exploiting on-chip MDM optical parametric devices and nonlinear optical signal processing applications.

References

[1] Z Xing *et al.*, "Waveguide-integrated graphene spatial mode filters for on-chip mode-division multiplexing," *Opt. Express*, vol. 27, no. 14, pp. 19188–19195, Jun. 2019.

[2] C. Gui, Y. Gao, Z. Zhang, and J. J. I. P. J. Wang, "On-chip silicon two-mode (de) multiplexer for OFDM/OQAM data transmission based on grating-assisted coupler," *IEEE Photon. J.*, vol. 7, no. 6, Dec. 2015, Art. no. 7905807.

[3] F. Ren *et al.*, "Cascaded mode-division-multiplexing and time-division-multiplexing passive optical network based on low mode-crosstalk FMF and mode MUX/DEMUX," *IEEE Photon. J.*, vol. 7, no. 5, Oct. 2015, Art. no. 7903509.

[4] G. Lu, K. S. Abedin, and T. Miyazaki, "All-optical RZ-DPSK WDM to RZ-DQPSK phase multiplexing using four-wave mixing in highly nonlinear fiber," *IEEE Photon. Technol. Lett.*, vol. 19, no. 21, pp. 1699–1701, Oct. 2007.

[5] Y. Tan, H. Wu, and D. Dai, "Silicon-based hybrid (de) multiplexer for wavelength-/polarization-division-multiplexing," *J. Lightw. Technol.*, vol. 36, no. 11, pp. 2051–2058, Nov. 2018.

[6] Z. Chen, Y. Zhu, X. Ruan, Y. Li, Y. Li, and F. Zhang, "Bridged coupler and oval mode converter based silicon mode division (De) multiplexer and terabit WDM-MDM system demonstration," *J. Lightw. Technol.*, vol. 36, no. 13, pp. 2757–2766, Mar. 2018.

[7] C. P. Chen *et al.*, "Mode and polarization multiplexing in a si photonic chip at 40Gb/s aggregate data bandwidth," *IEEE Photon. Technol. Lett.*, vol. 27, no. 1, pp. 22–25, Sep. 2015.

[8] B. Stern *et al.*, "On-chip mode-division multiplexing switch," *Optica*, vol. 2, no. 6, pp. 530–535, Jun. 2015.

[9] Y. Liu *et al.*, "Arbitrarily routed mode-division multiplexed photonic circuits for dense integration," *Nature Commun.*, vol. 10, pp. 1–7, Jul. 2019.

[10] X. Liu, R. M. Osgood Jr, Y. A. Vlasov, and W. M. Green, "Mid-infrared optical parametric amplifier using silicon nanophotonic waveguides," *Nature Photon.*, vol. 4, no. 8, pp. 557–560, May 2010.

[11] A. G. Griffith *et al.*, "Silicon-chip mid-infrared frequency comb generation," *Nature Commun.*, vol. 6, pp. 1–5, Feb. 2015.

[12] P. Marin-Palomo *et al.*, "Microresonator-based solitons for massively parallel coherent optical communications," *Nature*, vol. 546, no. 7657, pp. 274–279, Jun. 2017.

[13] C. Koos, L. Jacome, C. Poulton, J. Leuthold, and W. Freude, "Nonlinear silicon-on-insulator waveguides for all-optical signal processing," *Opt. Express*, vol. 15, no. 10, pp. 5976–90, May 2007.

[14] Z. Cheng, X. Chen, C. Y. Wong, K. Xu, and H. K. Tsang, "Mid-infrared suspended membrane waveguide and ring resonator on silicon-on-insulator," *IEEE Photon. J.*, vol. 4, no. 5, Aug. 2012.

[15] Q. Lin, J. Zhang, G. Piredda, R. W. Boyd, P. M. Fauchet, and G. P. Agrawal, "Dispersion of silicon nonlinearities in the near infrared region," *Appl. Phys. Lett.*, vol. 91, Jul. 2007, Art. no.021111.

[16] R. H. Khandokar, M. Bakaul, S. Skafidas, T. Nirmalathas, and M. Asaduzzaman, "Performance of planar, rib, and photonic crystal silicon waveguides in tailoring group-velocity dispersion and mode loss," *IEEE J. Sel. Top. Quantum Electron.*, vol. 22, no. 2, pp. 73–80, Sep. 2015.

[17] M. L. Cooper *et al.*, "Waveguide dispersion effects in silicon-on-insulator coupled-resonator optical waveguides," *Opt. Lett.*, vol. 35, no. 18, pp. 3030–3032, Sep. 2010.

[18] L. Zhang, Y. Yue, R. G. Beausoleil, and A. E. Willner, "Analysis and engineering of chromatic dispersion in silicon waveguide bends and ring resonators," *Opt. Express*, vol. 19, no. 9, pp. 8102–8107, Apr. 2011.

[19] A. C. Turner *et al.*, "Tailored anomalous group-velocity dispersion in silicon channel waveguides," *Opt. Express*, vol. 14, no. 10, pp. 4357–4362, May 15, 2006.

[20] S. Mas, J. Caraquitena, J. V. Galán, P. Sanchis, and J. Martí, "Tailoring the dispersion behavior of silicon nanophotonic slot waveguides," *Opt. Express*, vol. 18, no. 20, pp. 20839–20844, Sep. 2010.

[21] K. Y. Yang *et al.*, "Broadband dispersion-engineered microresonator on a chip," *Nature Photon.*, vol. 10, no. 5, pp. 316–320, Mar. 2016.

[22] Z. Jafari and F. Emami, "A silicon waveguide for tailoring dispersion of transverse electric and magnetic modes," *IEEE Photon. Technol. Lett.*, vol. 26, no. 9, pp. 885–888, May 2014.

[23] M. Yu, Y. Okawachi, A. G. Griffith, N. Picqué, M. Lipson, and A. L. Gaeta, "Silicon-chip-based mid-infrared dual-comb spectroscopy," *Nature Commun.*, vol. 9, pp. 1–6, May 2018.

[24] N. Singh "Octave-spanning coherent supercontinuum generation in silicon on insulator from 1.06 μm to beyond 2.4 μm," *Light: Sci. Appl.*, vol. 7, no. 1, pp. 17131–17131, Sep. 2018.

[25] Z. Li, H. Liu, N. Huang, Z. Wang, and J. Han, "Frequency-degenerate phase-sensitive optical parametric amplification based on four-wave mixing in graphene–silicon slot waveguide," *Appl. Phys. Express*, vol. 11, no. 6, May 2018, Art. no. 062201.

[26] C. Peucheret, Y. Ding, J. Xu, F. Da Ros, A. Parini, and H. Ou, "Signal processing for On-Chip space division multiplexing," in *Proc. Opt. Soc.Amer. Int. Conf. Adv. Photon.*, p. SpT2E.3, 2015.

[27] D. Vermeulen *et al.*, "High-efficiency fiber-to-chip grating couplers realized using an advanced CMOS-compatible silicon-on-insulator platform," *Opt. Express*, vol. 18, no. 17, pp. 18278–18283, Aug. 2010.